

IRON BULK AMORPHOUS ALLOY COATING FOR
REDUCED WEAR DAMAGE OF TURBINE
SURFACES

BY STAN DITTRICK

PHD CANDIDATE AT WASHINGTON STATE UNIVERSITY

ADVISOR AMIT BANDYOPADHYAY

DECEMBER, 31 2013

FOR THE HYDRO RESEARCH FOUNDATION

INTRODUCTION

Erosion and cavitation damage to hydro turbine blades is expensive. In 1999, dollars turbine damage can cost 15k to over 100k for repair work depending on turbine size. Unfortunately this is not the major cost of turbine damage. Lost power production is the major expense this downtime can cost upward of \$50/MW Hour of lost power production (1). With typical repair times of 2 to 4 weeks lost power production can become very expensive. There are other cost not included in this estimate which are harder to quantify. They include lost efficiencies of the turbine and a reduced blade life which can exceed a 30% reduction (2)

Silt in the water acts as an abrasive agent eroding the surface. Erosion of the turbine blade is divided into two types – (1) erosion caused by impact perpendicular to the blade and (2) erosion caused by a mostly parallel impact. In real world applications erosion is caused by some combination of these two types however it is useful to consider them separately. For parallel erosion the silt grinds along the surface. The most effective material for resisting this type of erosion is a hard material. In perpendicular erosion the particulates impact the surface. These impacts cause the turbine surface to break up. Since hard crystalline materials are usually brittle, a harder material is not always better. A tougher material is used to resist this type of erosion. Therefore, to resist both types of wear, the ideal material should be both harder as well as tougher.

The other source of damage to turbine blades is cavitation. Cavitation is caused by rapid changes in local pressure in a hydraulic fluid such as water. This phenomenon occurs near the trailing surfaces of turbine blades where the low pressure causes the liquid to vaporize. This creates a bubble which implodes violently as the pressure increases dramatically. This implosion

causes damage to the turbine blade which is similar to perpendicular erosion. Such types of blade damage can be minimized by making the surface tougher. Therefore the desired material for both erosion and cavitation resistance is also harder and tougher.

In the low temperature regime that hydraulic turbines operate, the toughest materials are going to be those with the smallest grain size and hence reduced slip plane motion. The extreme condition of smallest grain size is no grains at all in other words amorphous materials.

Unfortunately metals readily form highly ordered crystalline structures and until recently had to be cooled from liquid temperatures to room temperature in micro seconds to form amorphous materials. This only allowed for a very thin coating and required difficult processing steps to achieve amorphous coatings (3). More recent research results have shown that the introduction of a large number of metals with different atomic radii makes incorporation into a crystal structure more difficult (4). This significantly increases the time required for an alloy to crystallize. This makes it easier to cool the material fast enough to freeze the amorphous structure in place.

Another advancement in amorphous metal technology is a processing method which can create the high temperature gradients required to cool the material fast enough to retain the amorphous structure. This processing method is sometimes referred to as laser based additive manufacturing or free form fabrication among other names. Whatever it is called it utilizes localized laser heating to melt the metal powder. Only a small portion of the part is at melting temperatures, referred to as the melt pool, and the rest of the part remains relatively cool. This melt pool can cool much faster than the bulk of an entire part. Not only is the volume of the melt pool much smaller than a bulk part but the completed portion of the part and the base plate act as a heat sink. The final result shows that these new alloys can cool quick enough to avoid crystallization and maintain their amorphous nature or only partially crystallize (5).

Experimental

Samples were made from NanoSteel NSSHs7574 Super Hard Alloy Steel Powder from the NanoSteel Company Inc., Idaho Falls, ID. This powder contained Cr<25 Mo<15 W<10 C<3 Mn<5 Si<2 B<5 Fe balance with powder particles between 53 μm and 180 μm . Samples were made using a LENS™ 750 (Optomec Inc., Albuquerque NM) free form fabrication machine. Prior to fabrication NanoSteel powder was placed in the hopper. An inert carrier gas, in this case argon, delivered the powder to the focal point of the 750 watt continuous wave Nd:YAG laser. Even though the laser was rated at 750 watts the maximum power available to melt the powder was 500 watts after optic losses inside the machine. All samples were made with the laser set to deliver 400 watts. The powder melted to form a melt pool and a 3 axis gantry system moved the build plate in a raster motion to form each layer of the 3 dimensional part. It was more natural to think of a moving laser/melt pool rather than a moving part so it will be described in this manner. The scan speed of the laser was set to 122 cm/min. For all samples except compression samples hatch distance and layer thickness were set to 0.508 mm. For all samples except compression samples 15 mm by 15 mm hexahedron samples were made and cut with a diamond saw into 5 mm slices. Sample surfaces were prepared by grinding with 120 grit silica paper until the sample was flat and smooth then grinding with 320 grit, 600 grit and 1000 grit silica paper successively. Samples were then polished with 1 μm , 0.3 μm and 0.05 μm alumina polishes successively. Samples were then cleaned by soaking in methanol and placed in an ultrasonic bath for 5 minutes.

Compression samples varied from the other samples in both shape and processing parameters. Compression samples were prepared in 8mm diameter cylinders that were cut into 16mm long pieces. For compression samples hatch distance was varied between 0.508 mm and

0.762 mm in 0.127 mm increments. Layer thickness was varied between 0.508 mm and 0.889 mm in 0.127 mm increments. All samples were tested on a 50,000 lb. test frame. The modulus was determined by visually identifying the linear region of each plot disregarding both the initial ramp up region where the frame first engages the sample and the plastic zone where permanent deformation begins to occur. Hardness testing was conducted on a Shimadzu, HMV-2T, Japan with a 9.807 N load applied for 30 seconds. The average and standard deviation of ten samples was reported.

Wear testing was done on a Nanovea tribometer Irvine, California using a linear reciprocating pin on disk mode. Three mm Al_2O_3 bearings were used as “pins” on the sample “disks”. Testing was conducted at room temperature with a 1200 mm/min speed for a total wear distance of 1 km. The machine was set to 10 mm track length. Prior to testing the pin arm force sensor was calibrated with a 10 N weight. Prior to each test the pin arm was leveled and balanced. After balancing a 10 N load was added to the pin arm. The sensor was set to record force and distance every 200 μs . unfortunately this rate slowed down with data acquisition until at the end of the run it was as slow as every 1.75 sec. In order to identify the true zero the average was taken and all values were offset by this amount. This was possible because negative values just indicate direction and with a dataset of between 114000 and 122000 data points it is assumed there are as many at each position in the cycle above and below the curve. The coefficient of static friction was the peak of each cycle and it was not possible to definitively determine the exact location of each point in the cycle so an approximation was used. For every one thousand data points, the absolute value of the ten largest numbers were averaged and recorded as the value at the last distance in the group. This method was used to chart the coefficient of friction as it changed with sliding distance.

Results and Discussion

The wear rate for BAA was $1.2 \times 10^{-5} \pm 0.7 \times 10^{-5} \text{ mm}^3 / \text{N m}$ for a sliding distance of 1000m. This was a low wear rate. This low wear rate was expected due to the high Vickers hardness of 1015 ± 15 . The wear rate of 410 stainless steel was almost double that of BAA at $3.2 \times 10^{-5} \pm 0.8 \times 10^{-5} \text{ mm}^3 / \text{N m}$. The Vickers hardness of 410 stainless steel was less than the hardness of BAA by a factor of 5. With such a low Vickers hardness of 214 ± 3 , it was unexpected that the wear rate was not higher. While the wear rate was not inversely proportional to the hardness among similar materials, a large decrease in hardness usually corresponds to a large increase in the wear rate. The deviation from this pattern was attributed to a number of factors. While both materials were iron based, BAA had only 35% iron where 410 stainless steel was 84% iron. While most of the rest of the material in 410 stainless steel was chromium at 13.5%, in BAA the 25% chromium content meant a substantial percentage of the material was other elements. In BAA these elements included molybdenum, tungsten, manganese, boron, carbon and silicon. Aside from the composition differences in these two materials, a microstructural difference also existed. BAA had an amorphous microstructure free of grain boundaries where 410 stainless steel had a martensitic crystalline structure. The wear rate of 316 stainless steel was $4.9 \times 10^{-5} \pm 2.2 \times 10^{-5} \text{ mm}^3 / \text{N m}$ with a Vickers hardness of 185 ± 3 . The 53% increase in the wear rate for 316 stainless steel was more closely matched to the 14% drop in hardness when compared to 410 stainless steel. This made sense due to the major composition changes between 316 and 410 stainless steels were an increase in chromium to about 18.5% and the addition of 14% nickel in 316 stainless steel. The microstructure of 316 stainless steel was austenitic which while a different structure than martensite was still crystalline in nature.

The static coefficient of friction was plotted after an initial break in period of 500m. It might seem as though this was the dynamic coefficient of friction since the pin was sliding on the disk. The pin did not slide around in a circle at a constant speed this would be linear motion. In this experiment the pin slid along the track then slowed down and eventually stopped at the end of the track. While in reality the track moved and the pin was stationary it seemed more natural to talk about the pin moving. Either way the physical interaction of the pin and disk was the same. The pin was momentarily at rest then it quickly accelerated in the opposite direction until it started to slow down to stop at the opposite end. While sliding in one direction at a near constant speed the force on the arm was roughly constant. This constant force was the dynamic coefficient of friction. When the pin had almost stopped at the end of the track the force dropped off and fell to zero. At this point the pin was stationary. Without pause the force built in the opposite direction. At some point this force exceeded the static frictional forces and the pin began to move in the opposite direction. When this force was divided by the load it was the static coefficient of friction. Since the static frictional force exceeded the dynamic frictional force the static coefficient of friction was larger in magnitude than the dynamic coefficient of friction. Due to limits of the hardware no more than 6 data points were collected per cycle. While points near the center could be identified as due to the change in directions other points were impossible to discern. This was because points at the beginning of the directional change, points in the sliding dynamic frictional region and points in the static frictional region had a minimal difference in magnitude. This was true even though the contextual clues of large numbers of data points per cycle made these distinctions easy to make. The coefficient of static friction showed up as a peak where the dynamic coefficient showed up as a flat region after the static coefficient of friction peak. The directional change showed up as a fast transition between positive and negative values,

or vice versa. The coefficient of static friction for BAA increased slightly with time with a value close to 0.46 as shown in figure 1. There was little to no fluctuations in the coefficient for BAA. The coefficient of static friction for 316 stainless steel, which was also plotted in figure 1, was much higher ranging between 0.7 to 0.92. The coefficient of static friction, also shown in figure 1, for 410 stainless steel while higher in between 0.88 and 0.97 than 316 stainless steel. 410 stainless steel had substantially less variation than 316 stainless steel.

The layer height and hatch distance were adjusted for BAA and compressive strengths were adjusted in order to optimize processing parameters for building BAA samples. From these samples compressive tests were conducted. Compressive strength and modulus were determined with results listed in table 2. The first three adjustments of the layer height and hatch distance were in tandem. These tests revealed that samples with 0.51 mm and 0.64 mm layer thickness and hatch distances had the same compressive strength at 1650 MPa and similar Modulus values near 27 GPa as shown in figure 2. In fact, most of the compressive strength values were 1650 MPa though some differences in standard deviations were observed. Processing parameters that produced parts with a compressive strength less than 1650 were considered to produce a lower quality part. The next series shown in figure 3 maintained the hatch distance at 0.64 mm and adjusted the layer height. Looking only at the compressive strength the layer thickness could be as high as 0.76 mm. When the modulus was also considered the layer thickness of 0.76 had a low modulus 18GPa which eliminated this set of parameters. This indicated that parts made with a layer height and hatch distance of 0.64 mm could be used with results similar to those made at 0.51 mm with savings in processing time.

My original plan for testing of BAA only called for wear testing. Shortly after beginning the project however I realized that a more representative test for turbine blades would be

cavitation wear. A large portion of time I spent on this project I spent in this pursuit even though it was not included and hence not required for completion of my obligations to the Hydro-foundation. I found ASTM standard G134 Standard test method for erosion of solid materials by cavitating liquid jet and the associated adjunct which gave detailed prints for manufacture of the associated test apparatus. In addition to the jet portion a 21 MPa pump was required. Initially I was given an estimate of 2800 dollars for the device and I found a pump online for \$250 dollars. As I had no budget for this research I asked my advisor for funds. He asked me to rework the design to see if it could be made cheaper. I worked with the machinist and modified the design so it would be around \$1100 and I found a cheaper pump that cost \$100. I had the cavitation apparatus made and it is shown in figure 4. The basic device was simple a jet of water was directed into an obstruction which formed a low pressure bubbles in the shadow of the obstruction. The collapse of these low pressure bubbles was cavitation. I used an adjustable speed DC motor that I borrowed from another lab at Washington State University and tank that I found in the lab the setup as was shown in figure 5. I needed to attach the pump to the motor so I designed a bracket and wheel using Solidworks and built those parts using our Titan rapid prototyping machine. These parts were the white plastic parts shown in the figure. I purchased the high pressure hose and some of the fittings with my own funds. During some initial testing of the device I blew out one of the viewing windows so I purchased a safety relief valve and a pressure gauge for the internal water pressure. These items were not shown in the picture. After a few minutes of running the pump lost pressure so I got a replacement. After a few minutes, the replacement pump also lost pressure. The vender claimed that while the pump was rated at 3500 psi that was not supposed to be continuous pressure. The pump never exceeded 1800 psi but that is not important part, I needed a better pump. The pumps I found were several thousand dollars.

In my search I realized that pressure washers get to high pressures and are much cheaper. Inexpensive electric pressure washers max out at 2000psi. Higher pressure units start around \$1800. Since I did not have funds for that I decided to try a 2000psi unit. Unfortunately after 48 hours of testing on one sample I was not able to cause detectable wear with the pressure washer. Since the materials I used are tough materials I tried aluminum just to show proof of concept. I found no damage on aluminum. I am confident that with the correct pump I would have found wear damage in this time frame. Running the experiment for an extended period of two weeks or more would also result in wear damage.

I decided to try something else. Though the damage caused by ultrasound cavitation does not correlate well to damage caused by jet cavitation I borrowed a high powered ultrasound cavitation device. While it quickly removed some paint from my test sample after 24 hours, there was no discernible cavitation damage. After I spent substantially more than allotted by my professor and many hundreds of hours on this portion of my project which was not even part of my approved project, I was forced to stop working on this portion of the project. While the cavitation testing did not produce reportable research results it was an educational experience. Design fabrication and assembly of the test apparatus was more complex and took far longer than expected.

Bibliography

1. *Hydro turbine profitability and cavitation erosion*. **al, Paul Bordon et.** s.l. : ASCE, 1999. Vol. 76.
2. *Cavitation Erosion in Hydroturbines*. **al., Roger E. A. Arndt et.** 10, s.l. : ASCE, 1989, Vol. 115, p. 1297.
3. *Non-crystalline Structure in Solidified Gold–Silicon Alloys* . **K. Klement, R. H. Willens, P. Duwez.** 1960, Nature, Vol. 187, p. 869.
4. **T. Egami, Y. Waseda.** 1984, Journal of Non-Crystalline Solids, Vol. 64, p. 113.
5. *Laser Processing of Fe-Based Bulk Amorphous Alloy Coatings on Titanium*. **Himanshu Sahasrabudhe, Stanley A. Ditrack & Amit Bandyopadhyay.** s.l. : Springer, 2013, Metallurgical and Materials Transactions A, pp. DOI: 10.1007/s11661-013-1846-0.

Table 1: Wear rate and Vickers hardness for BAA, 410 SS and 316 SS

	Wear Rate $\text{mm}^3 / \text{N m}$	Vickers Hardness (HV)
BAA	$1.2 \times 10^{-5} \pm 0.7 \times 10^{-5}$	1015 \pm 15
410 SS	$3.2 \times 10^{-5} \pm 0.8 \times 10^{-5}$	214 \pm 3
316 SS	$4.9 \times 10^{-5} \pm 2.2 \times 10^{-5}$	185 \pm 3

Table 2: Modulus and compressive strength of BAA at variable layer heights and hatch distances

Height of Layer mm	Hatch Distance mm	Modulus MPa	Compressive Strength MPa
0.51	0.51	27000+/-3000	1650+/-20
0.64	0.64	26000+/-2000	1650+/-90
0.76	0.76	18700+/-400	1400+/-200
0.51	0.64	21000+/-3000	1650+/-100
0.64	0.64	26000+/-2000	1650+/-90
0.76	0.64	18000+/-3000	1650+/-80
0.89	0.64	21000+/-2000	1590+/-50

Figure 1: Coefficient of friction per sliding distance for BAA, 410 SS and 316 SS

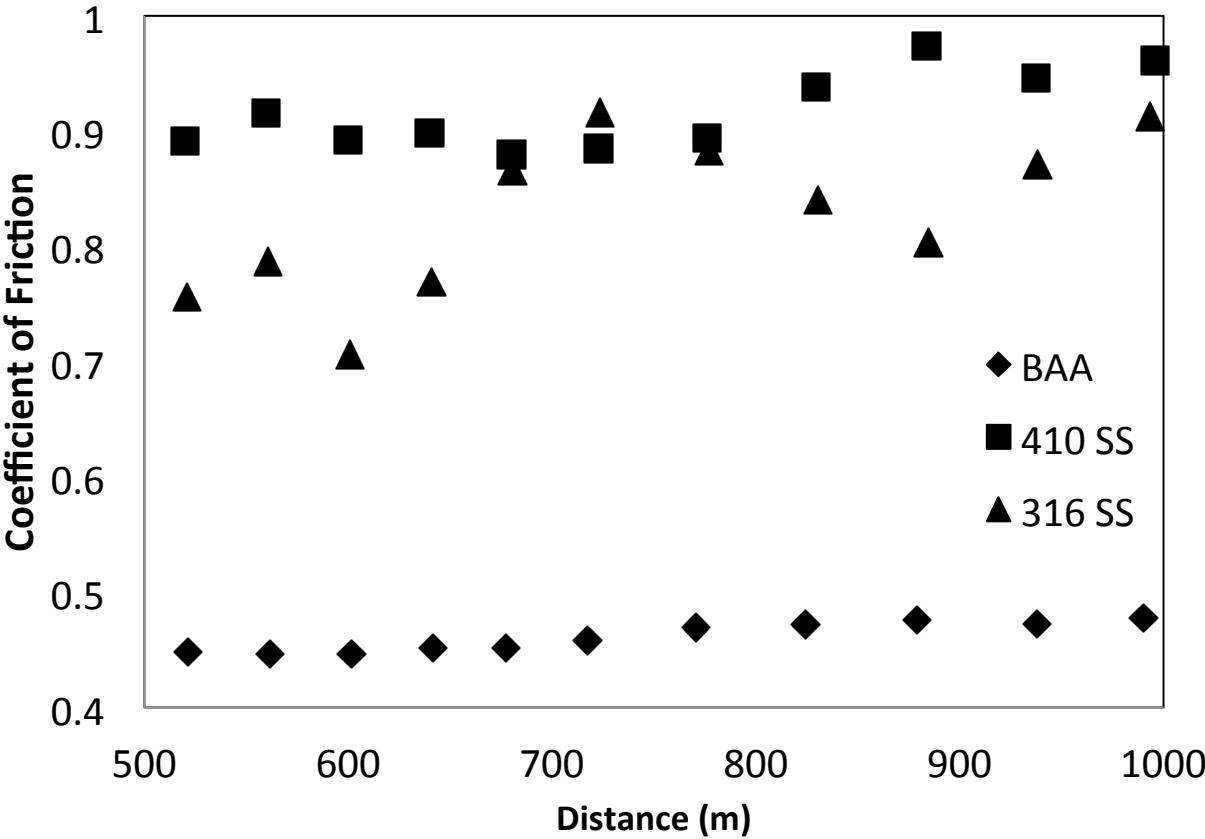


Figure 2: Stress strain curve of BAA processed with the same layer height as hatch distance as listed

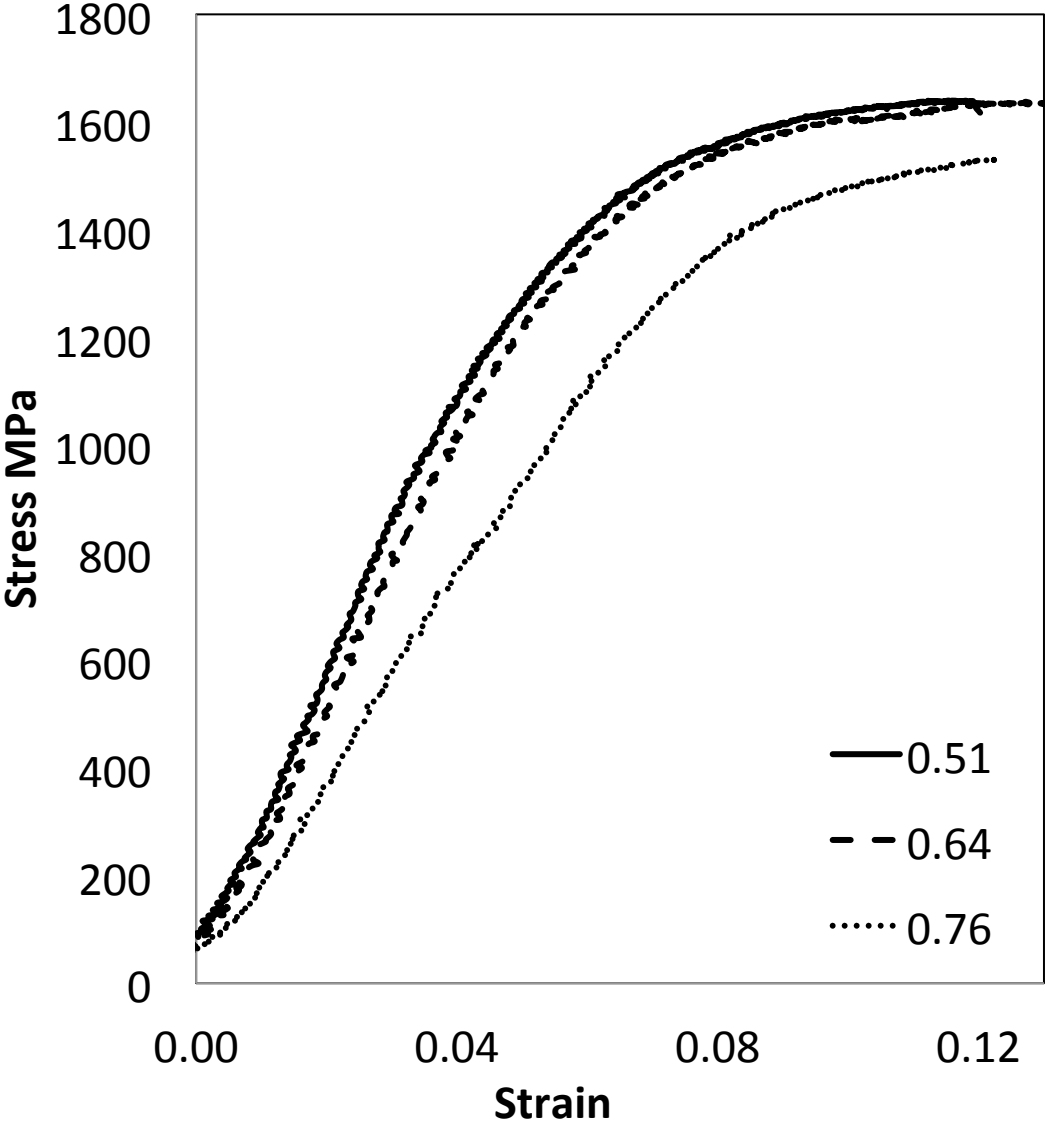


Figure 3: Stress strain curve of BAA processed with different layer thicknesses as listed

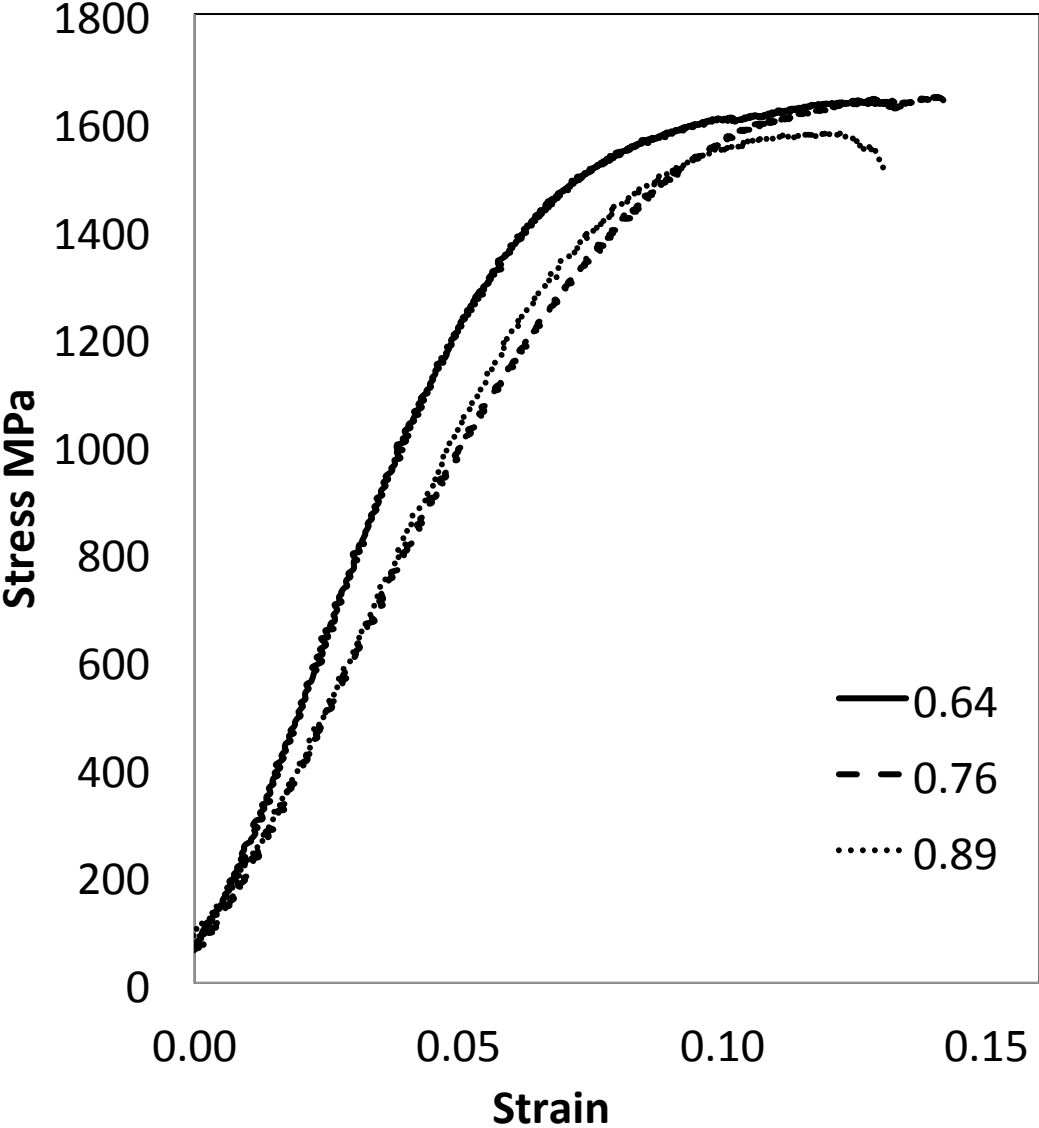


Figure 4: Cavitation wear test apparatus

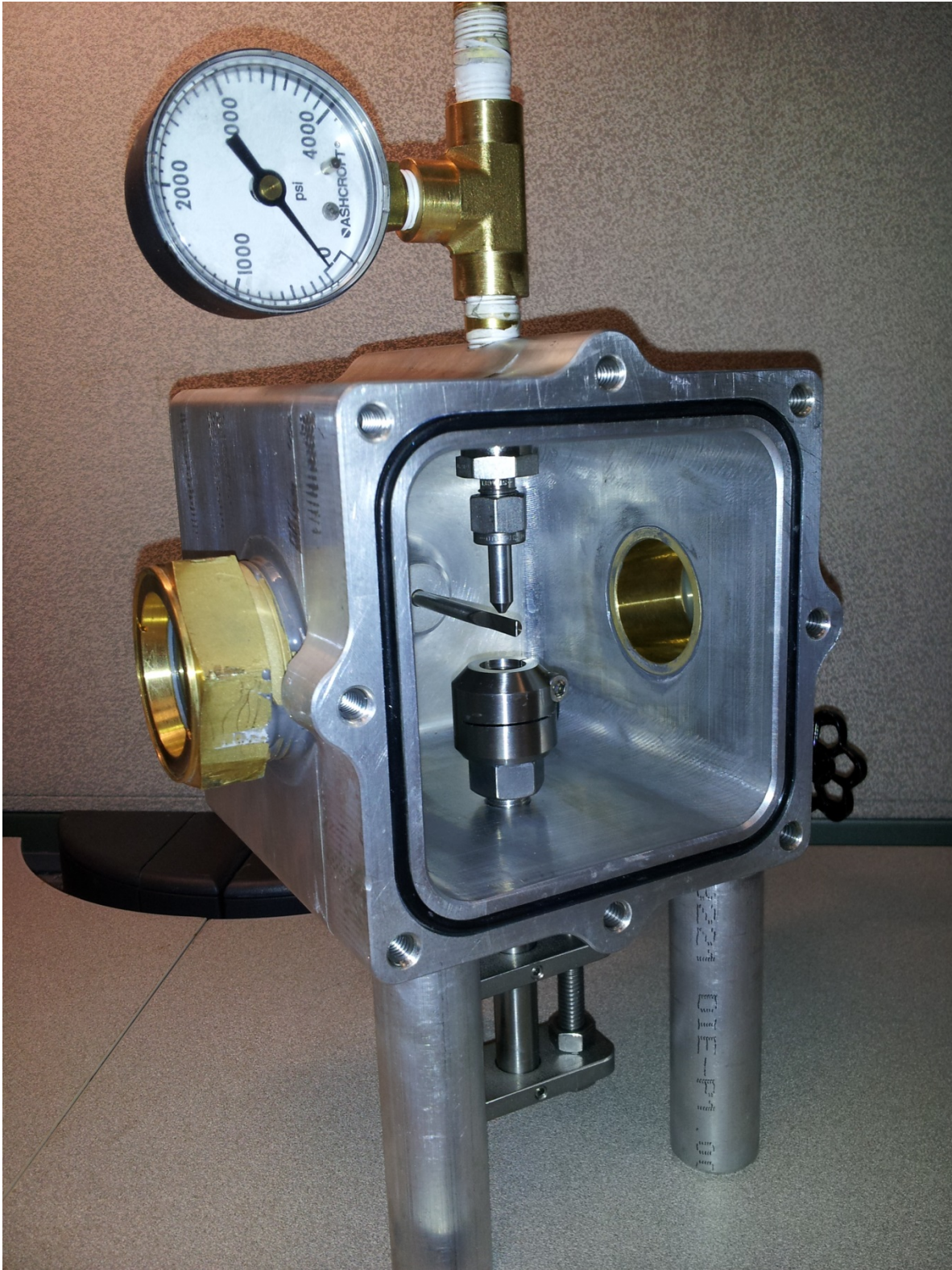


Figure 5: Cavitation testing apparatus with auxillary devices

